

# Shear stress mapping in microfluidic devices by optical tweezers

Jing Wu,<sup>1,2,4</sup> Daniel Day,<sup>1,3,\*</sup> and Min Gu<sup>1</sup>

<sup>1</sup>Centre for Micro-Photonics, Faculty of Engineering and Industrial Sciences, Swinburne University of Technology, Hawthorn, PO Box 218, Victoria 3122, Australia

<sup>2</sup>Department of Optical Engineering, Zhejiang University, Hangzhou 310027, P. R. China

<sup>3</sup>Cooperative Research Centre for Polymers, Notting Hill, Victoria 3168, Australia

<sup>4</sup>jingcindywu@126.com

\*dday@swin.edu.au

**Abstract:** We present an optical tweezer sensor for shear stress mapping in microfluidic systems of different internal geometries. The sensor is able to measure the shear stress acting on microspheres of different sizes that model cell based biological operations. Without the need for a spatial modulator or a holographic disk, the sensor allows for direct shear stress detection at arbitrary positions in straight and curved microfluidic devices. Analytical calculations are carried out and compared with the experimental results. It is observed that a decrease in the microsphere size results in an increase in the shear stress the particle experiences.

©2010 Optical Society of America

**OCIS codes:** (350.4855) Optical tweezers or optical manipulation; (280.4788) Optical sensing and sensors; (130.6010) Sensors.

---

## References and links

1. R. G. Larson, *The structure and rheology of complex fluids* (Oxford U. Press, 1998).
2. A. Sin, S. K. Murthy, A. Revzin, R. G. Tompkins, and M. Toner, "Enrichment using antibody-coated microfluidic chambers in shear flow: model mixtures of human lymphocytes," *Biotechnol. Bioeng.* **91**(7), 816–826 (2005).
3. M. Greiner, P. Carter, B. Korn, and D. Zink, "New approach to complete automation in sizing and quantitation of DNA and proteins by the automated lab-on-a-chip platform from Agilent Technologies," *Nat. Methods* **1**(1), 87–89 (2004).
4. P. S. Dittrich, and A. Manz, "Lab-on-a-chip: microfluidics in drug discovery," *Nat. Rev. Drug Discov.* **5**(3), 210–218 (2006).
5. D. Wirtz, "Particle-tracking microrheology of living cells: principles and applications," *Annu Rev Biophys* **38**(1), 301–326 (2009).
6. H. Mao, T. Yang, and P. S. Cremer, "A microfluidic device with a linear temperature gradient for parallel and combinatorial measurements," *J. Am. Chem. Soc.* **124**(16), 4432–4435 (2002).
7. G. Pesce, A. Sasso, and S. Fusco, "Viscosity measurements on micron-size scale using optical tweezers," *Rev. Sci. Instrum.* **76**(11), 115105 (2005).
8. R. R. Brau, J. M. Ferrer, H. Lee, C. E. Castro, B. K. Tam, P. B. Tarsa, P. Matsudaira, M. C. Boyce, R. D. Kamm, and M. J. Lang, "Passive and active microrheology with optical tweezers," *J. Opt. A: Pure Appl. Opt.* **9**(8), S103–S112 (2007).
9. E. Eriksson, J. Scrimgeour, J. Enger, and M. Goksor, "Holographic optical tweezers combined with a microfluidic device for exposing cells to fast environmental changes," *Proc. SPIE* **6592**, 65920P (2007).
10. H. Mushfique, J. Leach, H. Yin, R. Di Leonardo, M. J. Padgett, and J. M. Cooper, "3D mapping of microfluidic flow in laboratory-on-a-chip structures using optical tweezers," *Anal. Chem.* **80**(11), 4237–4240 (2008).
11. A. Ashkin, "Forces of a single-beam gradient laser trap on a dielectric sphere in the ray optics regime," *Biophys. J.* **61**(2), 569–582 (1992).
12. W. Chester, D. R. Breach, and I. Proudman, "On the flow past a sphere at low Reynolds number," *J. Fluid Mech.* **37**(04), 751 (1969).
13. Y. Inouye, S. Shoji, H. Furukawa, O. Nakamura, and S. Kawata, "Pico-Newton friction force measurements using a laser-trapped microsphere," *Jpn. J. Appl. Phys.* **37**(Part 2, No. 6A), L684–L686 (1998).
14. C. T. Nguyen, F. Desgranges, G. Roy, N. Galanis, T. Mare, S. Boucher, and H. Angue Mintsu, "Temperature and particle-size dependent viscosity data for water-based nanofluidics - hysteresis phenomenon," *Int. J. Heat Fluid Flow* **28**(6), 1492–1506 (2007).
15. P. Becher, *Encyclopedia of emulsion technology* (Marcel Dekker Inc., 1996).
16. J. V. Green, T. Kniazeva, M. Abedi, D. S. Sokhey, M. E. Taslim, and S. K. Murthy, "Effect of channel geometry on cell adhesion in microfluidic devices," *Lab Chip* **9**(5), 677–685 (2009).

## 1. Introduction

For years the study of fluid systems relied on conventional rheometers, which can only be applied to smaller systems as an external coupling component with poor resolving ability for localised changes [1]. As more fluid-based biological processes are now being performed on micrometer scale platforms in the past decade [2–4], the research on specific rheological detectors for microsystems has become one of the most sought-after topics in sensing. Existing techniques such as particle tracking video-microrheology [5] and fluorescence recovery after photobleaching [6] would either alter the fluid properties (e.g. viscosity) or require extensive mathematical corrections. Due to the non-invasive nature and highly localized sensing of optical tweezers, there has been an interest to use them in microrheology (usually for viscosity measurements) [7,8]. They have recently been demonstrated as fluid sensors in microfluidic environments [9,10]. Nevertheless, to date there has been quite limited work on shear stress sensing in microfluidic systems. Considering the fact that shear stress can determine the morphological characteristics and internal physiology of the cells, a shear stress sensor specifically for microfluidic systems would be of great importance in life sciences. Potential applications would be in the study of cell adhesion and cell mechanics on microfluidic chips.

In this work we present an optical tweezer sensor for shear stress mapping in microfluidic systems of different internal geometries. By direct measurement of Stokes force acting on optically trapped microspheres, we are able to achieve shear stress measurement at arbitrary positions in microfluidic channels. Measurements are realized without the need of a spatial modulator or a holographic disk, with which the trapping stiffness and system error are influenced by the step of the modulation in regard to the particle size. Another merit from the simplified configuration is that it does not require comparably large quantitative measurements. Characterization of the shear stress with microspheres of different sizes is performed, including particles of 5-15  $\mu\text{m}$ , which is a size range that many cells fall into. The shear stress distributions across a straight channel are measured and compared with analytical calculations. Boundary correction is considered to compensate for bias from proximity surface effect. After the proof-of-concept measurements, the shear stress distribution is mapped in a curved microfluidic channel.

## 2. Experiment

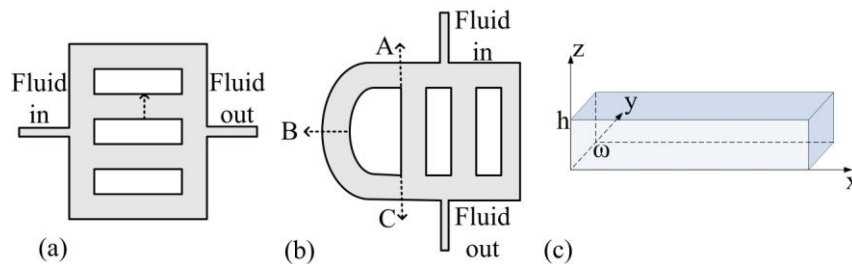


Fig. 1. Multichannel devices with (a) straight channels and (b) a u-shaped channel. The dashed lines indicate the directions of the measurements. (c) An illustration of the microfluidic channel with a rectangular cross-section.

The microfluidic devices used in our experiments were fabricated in poly (dimethyl siloxane) (PDMS) by soft lithography. The master templates were cut out in laminated films using a  $\text{CO}_2$  laser (Universal Laser Systems). An illustration of the microfluidic devices fabricated is presented in Fig. 1(a) and (b). The straight channel device with four straight channels (height  $h = 120 \mu\text{m}$ , width  $w = 4 \text{ mm}$ ) and the u-shaped channel device ( $h = 120 \mu\text{m}$ ,  $w = 2 \text{ mm}$ ) were mounted onto translation stage and tested for the volumetric flow rate  $Q$  before the sensor calibration. Afterwards the trapping efficiency with respect to different microsphere diameters was characterized for system calibration. Polystyrene microspheres suspended in de-ionized water were pumped through the straight microchannel. A femtosecond laser beam (800 nm,

82 MHz, 90 fs) was expanded and collimated before tightly focusing into a microfluidic channel through a 1.2 NA objective to form the optical tweezers. The laser power was set at 30 mW and any microsphere at the focus region was trapped and held against in the flow. The power was then reduced towards the trapping threshold power at which point the microsphere escaped. The threshold laser trapping power was recorded for microspheres of different sizes (5, 10 and 15  $\mu\text{m}$ ). At the same time, the trapping process was recorded by a CCD camera and the particle velocities were determined from the video by Image J. The particle velocities and laser trapping power were then used to calculate the trapping efficiency of the optical tweezers for the different microsphere sizes. The calibration result for the trapping efficiency for 5, 10 and 15  $\mu\text{m}$  microspheres were 0.07932, 0.105608 and 0.130454, respectively. With the same procedure as for the calibration, the shear stress inside the microfluidic devices was then characterized by measuring the optical trapping force required to trap the microspheres. The measurements were then taken at different transverse positions across the microfluidic channels (as shown in Fig. 1 (a) and (b) by the dashed lines).

### 3. Result and discussion

#### 3.1 Boundary correction in the experimental measurements

The optical trapping force is given by reference [11] as

$$F_t = \frac{Q_t n_2 P}{c}, \quad (1)$$

where  $F_t$  is the the trapping force,  $Q_t$  is the transverse trapping efficiency,  $n_2$  is the refractive index of the water,  $P$  is the threshold laser power,  $c$  is the speed of light in a vacuum. Boundary correction is considered to compensate for the proximity surface effect. The Stokes force ( $F_{drag}$ ) is defined in reference [12] as

$$F_{drag} \approx 6\pi\mu r v (1 + P_{b1}), \quad (2)$$

where  $\mu$  is the viscosity coefficient of the water,  $r$  is the microsphere radius,  $v$  is the flow velocity,  $P_{b1}$  is the boundary correction parameter for the bottom surface in the channel. Because we operated in a low Reynolds number condition and close to the bottom boundary, the effect of Reynolds number variation and the correction for the top surface are negligible.  $P_{b1}$  is given by reference [13] as

$$P_{b1} = \frac{1}{\left(1 - \frac{9}{16}\left(\frac{r}{h}\right) + \frac{1}{8}\left(\frac{r}{h}\right)^3 - \frac{4}{256}\left(\frac{r}{h}\right)^4 - \frac{1}{16}\left(\frac{r}{h}\right)^5\right)} - 1, \quad (3)$$

where  $h$  is the distance from the channel bottom surface to the center of the microsphere. When the Stokes force  $F_{drag}$  is balanced by optical force, the fluid velocity can be determined by the threshold optical trapping power.

#### 3.2 Theoretical calculations for the velocity and shear stress

For a Poiseuille flow with a constant density and non-slip boundary condition (shown in Fig. 1 (c)), one solution to the Navier-Stokes equations is denoted by

$$v_x(y, z) = \frac{-16\Delta P}{\pi^4 \mu L} \sum_{n\_odd} \sum_{m\_odd} \frac{1}{nm \left(\frac{n^2}{\omega^2} + \frac{m^2}{h^2}\right)} \sin\left(\frac{n\pi}{w} y\right) \sin\left(\frac{m\pi}{h} z\right), \quad (4)$$

where  $v_x(y, z)$  is the flow velocity at position  $(y, z)$ ,  $\Delta P$  is the pressure drop in the channel,  $\mu$  is the fluid viscosity,  $L$  is the channel length.

The shear stress  $\tau$  is denoted by

$$\tau = \mu \frac{\partial v_x}{\partial z} \quad y, z. \quad (5)$$

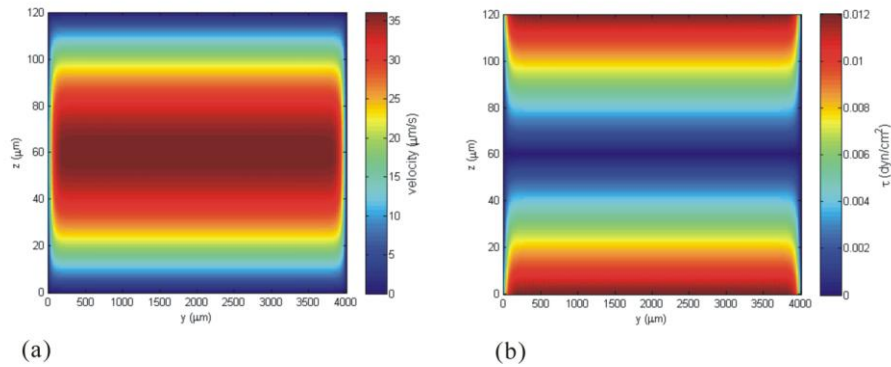


Fig. 2. Theoretical (a) flow velocity and (b) shear stress in the  $y$ - $z$  plane of the straight microfluidic channels ( $h = 120 \mu\text{m}$ ,  $w = 4 \text{ mm}$ ).

The calculated fluid velocity and shear stress in the straight channel on  $y$ - $z$  plane were shown in Fig. 2. The measured volumetric flow rate is  $1.1562384 \times 10^{-11} \text{ m}^3/\text{s}$ . The viscosity of water is  $0.001 \text{ Pa}\cdot\text{s}$ . The unit for shear stress is  $\text{dyn}/\text{cm}^2$  ( $1 \text{ dyn}/\text{cm}^2 = 0.1 \text{ Pa}$ ). As observed in Fig. 2 (a), along  $z$  direction, the flow moves at the highest velocity in the middle of the channel and decreases towards the top and bottom of the channel. Similarly, observation along  $y$  direction shows that the flow velocity decreases slowly from the center of the channel and drops sharply at the proximity of the side walls ( $y = 0$  and  $w$ ). Figure 2 (b) shows the shear stress in the straight channel on  $y$ - $z$  plane. The shear force increases from the middle of the channel towards both the top and bottom surfaces of the microchannel.

### 3.3 Comparison between experimental result and theoretical calculations

As shown in Fig. 3, the measured particle velocities and shear stress acting on different microspheres (the colored symbols) are compared to the calculated fluid velocity and shear stress (the solid lines) inside a straight microfluidic channel. Data is extracted from the two-dimensional calculations (shown in Fig. 2) in order to directly compare those results at the same vertical distance above the bottom surface of the channel. The theoretical calculation is fixed at a  $y$  position of  $20 \mu\text{m}$  above the bottom surface of the channel which corresponds to the height of the trapping experiments. The theoretical velocity was normalized by the average fluid velocity determined from the volumetric flow rate measurements. For particles with less than  $1 \mu\text{m}$  diameters, the experimental result would be significantly influenced by effects such as Brownian motion, which reduces the trapping stability and measurement accuracy. In these experiments we opted to use  $5$ ,  $10$  and  $15 \mu\text{m}$  microspheres over smaller ones because the size of many cells ranges from a few micrometers to tens of micrometer.

Comparison of the experimentally measured velocities of the  $5$ ,  $10$  and  $15 \mu\text{m}$  microspheres suggests that all the microparticles are moving at different velocities to the fluid (see Fig. 3(a)) and they actually experience different shear stress compared to the pure fluid system (see Fig. 3(b)). In addition, the measured microsphere velocity and shear stress profiles show parabolic profiles, with the maximum velocities and shear stresses at the channel center scaled down corresponding to the microsphere diameters. The smaller the scale of the microspheres, the wider range of velocity and shear stress they experience in the channel.

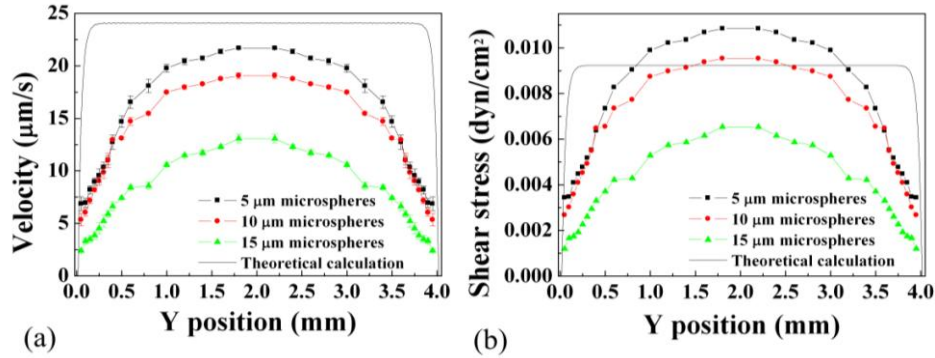


Fig. 3. Theoretical and experimental results for (a) fluid velocity and (b) shear stress, in the straight microfluidic channels ( $h = 120 \mu\text{m}$ ,  $w = 4 \text{ mm}$ ).

The major reason for the microsphere size dependence of shear stress could be that, when microparticles are added to the fluid system, the viscosity of the whole suspension become particle size dependent [14]. Given a constant particle mass in a suspension, a reduction in the microsphere size means a higher number of smaller particles in the suspension. This leads to more particle-particle interactions in the suspension and an increase in the flow resistance. As a result, the viscosity of the suspension system is increased. Because we were operating in the intermediate shear stress region, the particle-particle interactions are not negligible [15]. Besides, the variation of fluid velocity across the particle surfaces also attributes to the differences. In the region where trapping was performed (as shown in Fig. 4 (a)), the fluid velocity across the microsphere surface is not the same for the different sized microspheres at the same position (as shown in Fig. 4 (b)). The larger the diameter of the microsphere is, the larger the variation of fluid velocity is across the microsphere surface. As a result of the above effects, the effective shear stress acting on the microspheres is not the same as the theoretical value, and when smaller microparticles are added to the system, the actual shear stress may not be less than the theoretical shear stress of the fluid system. Thus, in biological or chemical operations, the addition of microparticles should be considered in theoretical simulations, and the real shear stress acting on the microparticles is affected by the microsphere size.

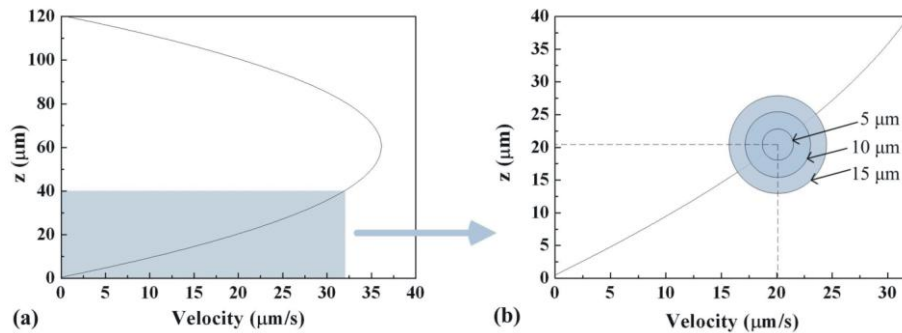


Fig. 4. (a) The theoretical fluid velocity along the  $z$  direction in the middle of the straight channel. (b) The fluid velocity represented by the shaded region in (a) and illustrations of microspheres of 5, 10 and 15  $\mu\text{m}$  diameter.

The experimental bias could be from several reasons, such as the effect of channel roughness of the sidewalls or the effect of microspheres that were stuck to the channel surface which perturb the flow profile. Thus the detection accuracy could be further enhanced by optimization of the sensor design and fabrication, or by appropriate surface treatment to reduce surface adhesion in the channel.

With the development of microfluidic devices towards various applications, the internal geometries of those devices become more complex. For instance, it is reported that microfluidic devices with curved sections tend to provide more uniform and predictable cell adhesion on the surface than straight channels [16]. In our experiments, to better explore the performance of the optical tweezers for shear stress mapping in a real microfluidic environment, we also applied the method to a u-shaped channel.

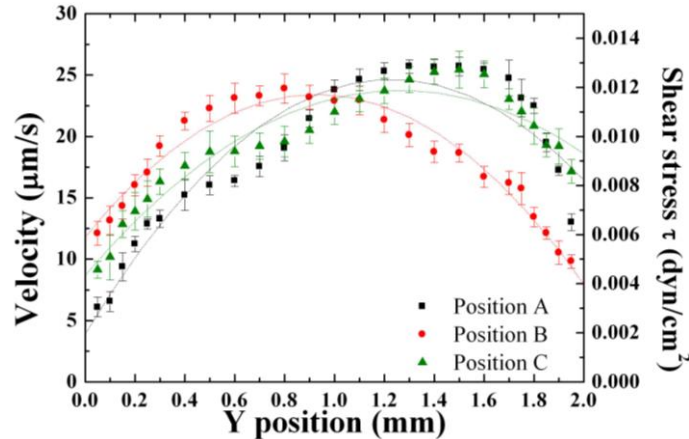


Fig. 5. The measured velocity and shear stress in a curved microchannel.

Measurements were taken at three different positions A, B and C (as shown in Fig. 1 (b)) using 5 µm microspheres. As shown in Fig. 5, the shear stress measurements at the start and end of the u-shaped channel (positions A and C from Fig. 1 (c)) are asymmetric, due to the branching geometry. It is a result of the flow from the adjacent channel that reduces the fluid velocity and shear stress on the inside of the channel. However, as the flow moves along the u-shaped bend, the fluid on the inside of the channel begins to move at a higher velocity, known as the ‘race track’ effect. This consequently results in the change in shear stress as well. The measurement at position B clearly demonstrates the increase in shear stress on the inside of the channel. Using optically trapped microspheres we were able to directly track the changing shear stress profile acting on the microspheres along the u-shaped channel.

#### 4. Conclusion

In summary, we have demonstrated an optical tweezer based microrheological sensor to map the shear stress in microfluidic devices of different geometries. The sensor is able to measure the shear stress acting on the microspheres of different sizes. The sensor is designed in a simple manner without the use of a spatial modulator or a holographic disk, and is able to operate with large microparticles of up to 15 micrometer. The detection of local shear stress acting on the microparticle of different sizes is performed. Comparison with analytical calculation indicates that microspheres were moving at different velocities to the fluid, and the shear stress acting on them is related to the microsphere size. After the proof-of-concept measurement in a straight microfluidic channel, the sensor is demonstrated for shear stress mapping in a curved microfluidic channel.

#### Acknowledgments

The authors would like to acknowledge Swinburne University of Technology through the Swinburne University Postgraduate Award and the Cooperative Research Centre for Polymer. Zhejiang University is Jing Wu's current address and her work in this paper was fully completed at Swinburne University of Technology.